EGU2016
3624

Fault-related Structural Permeability: Qualitative Insights of the Damage-Zone from Micro-CT Analysis.

Rodrigo Gomila [1,2*], Gloria Arancibia [1,2], Mathias Nehler [3], Rolf Bracke [3], Ferdinand Stöckhert [3].

1. Departamento de Ingeniería Estructural y Geotécnica, Pontificia Universidad Católica de Chile, Santiago, Chile.
2. Andean Geothermal Centre of Excellence (CEGA, FONDAP-CONICYT), Universidad de Chile, Santiago, Chile.
3. Laboratories of Geotechnologies and Seismic Observation. GZB – International Geothermal Center. Bochum University, Bochum, Germany.

* Corresponding author: ragomila@uc.cl

I. Introduction

Fault zones and their related structural permeability play a leading role in the migration of fluids through the continental crust. A first approximation to understanding the structural permeability conditions, and the estimation of its ancient hydraulic conditions (i.e. palaeo-permeability and fracture porosity) is the 2D analysis of its veinlets, usually made in thin-section. Those estimations are based in geometrical parameters, such as average fracture density, length and aperture, which can be statistically modelled assuming penny-shaped fractures of constant radius and aperture within an anisotropic fracture system. Thus, this model is related to fracture connectivity, its length and to the cube of the fracture apertures. In this way, the estimated values presents their own inaccuracies owing to the method used. Therefore, the study of the real spatial distribution of the veinlets of the fault-related fracture mesh (3D), feasible with the use of micro-CT analyses, is a first order factor to unravel both, the real structural permeability conditions of a fault-zone, together with the validation of previous estimations made in 2D analysis in thin-sections. This early contribution shows the preliminary results of a fault-related fracture mesh and its 3D spatial distribution in the damage zone of the Jorgillo Fault (JF).

II. Geological Framework

The Atacama Fault System (AFS) is a ca. 1000 km long trench-parallel large-scale structure (Figure 1). The well-documented left-lateral strike-slip movement has been interpreted as the result of the SE-ward oblique subduction of the Aluk (Phoenix) oceanic plate between 190 and 110 Ma. Recent activity of the AFS has been documented as extensional and interpreted as a reactivation of the system in response to mega-thrust earthquakes.

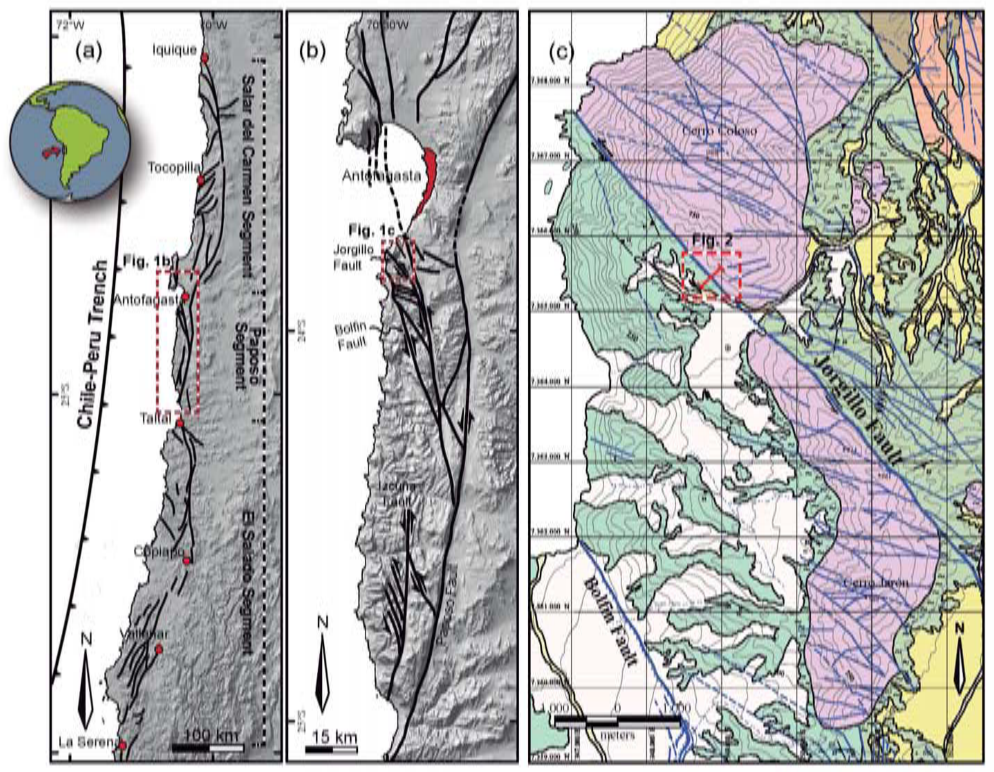

Figure 1:
(a) Simplified structural map of the Atacama Fault System.
(b) Simplified structural map of the central segment of AFS showing the main faults within.
(c) Regional geological map showing the Jorgillo Fault (blue bold line), main faults, geological units and transect location.

The Jorgillo Fault (JF) is a ca. 20 km long NNW striking strike-slip fault cutting Mesozoic rocks with sinistral displacement of ca. 4 km (Figure 1c). In the study area, the JF cuts through metadioritic and gabbroic rocks at the west (JFW) and the east side (JFE) (Figure 2), respectively. A 400 m fault perpendicular transect was mapped and sampled for structural analyses of the damage zone and protolith.

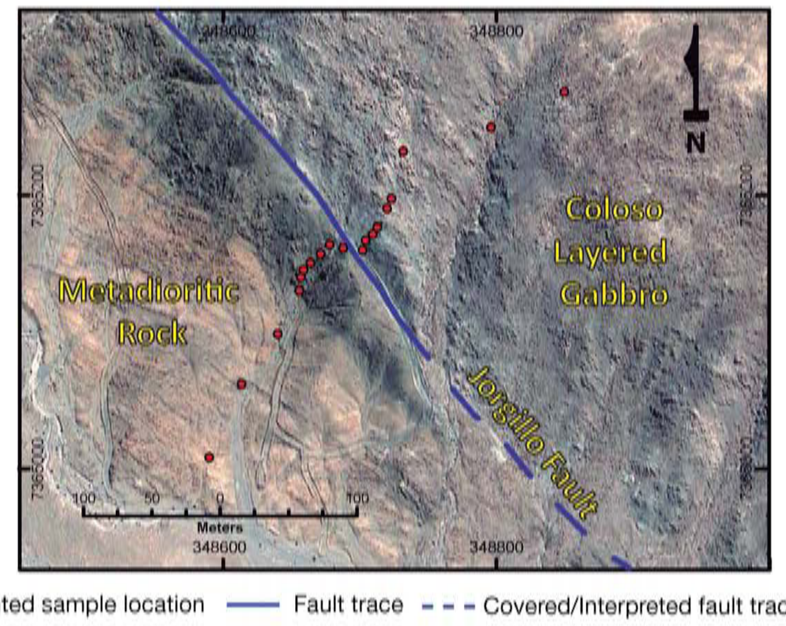

Figure 2:
Transect location, orthogonal to Jorgillo Fault's strike. Location of fault damage zone samples are shown.

III. Methodology

The methodology consisted of the drilling of vertically oriented plugs of 5 mm in diameter (Figure 3a and b) located at different distances from the JF core – damage zone boundary. Each specimen was, then, scanned with an x-ray micro-CT scanner (ProCon X-Ray CTalpha; Figure 3c) in order to assess the fracture mesh. X-rays were generated in a transmission target x-ray tube with acceleration voltages ranging from 90-120 kV and target currents from 40-60 μA. The focal spot size on the diamond/tungsten target was about 5 μm. The x-ray beam was filtered using a 1 mm Aluminum plate before passing the sample (Figure 3d). 1200 x-ray images were taken during a full rotation of the sample using an amorphous silicon flat panel detector with 1516x1900 pixels. This resulted in a voxel resolution of about 8 μm in the 3D data reconstructed from the images.

III.1 Sample Preparation and CT Set-up

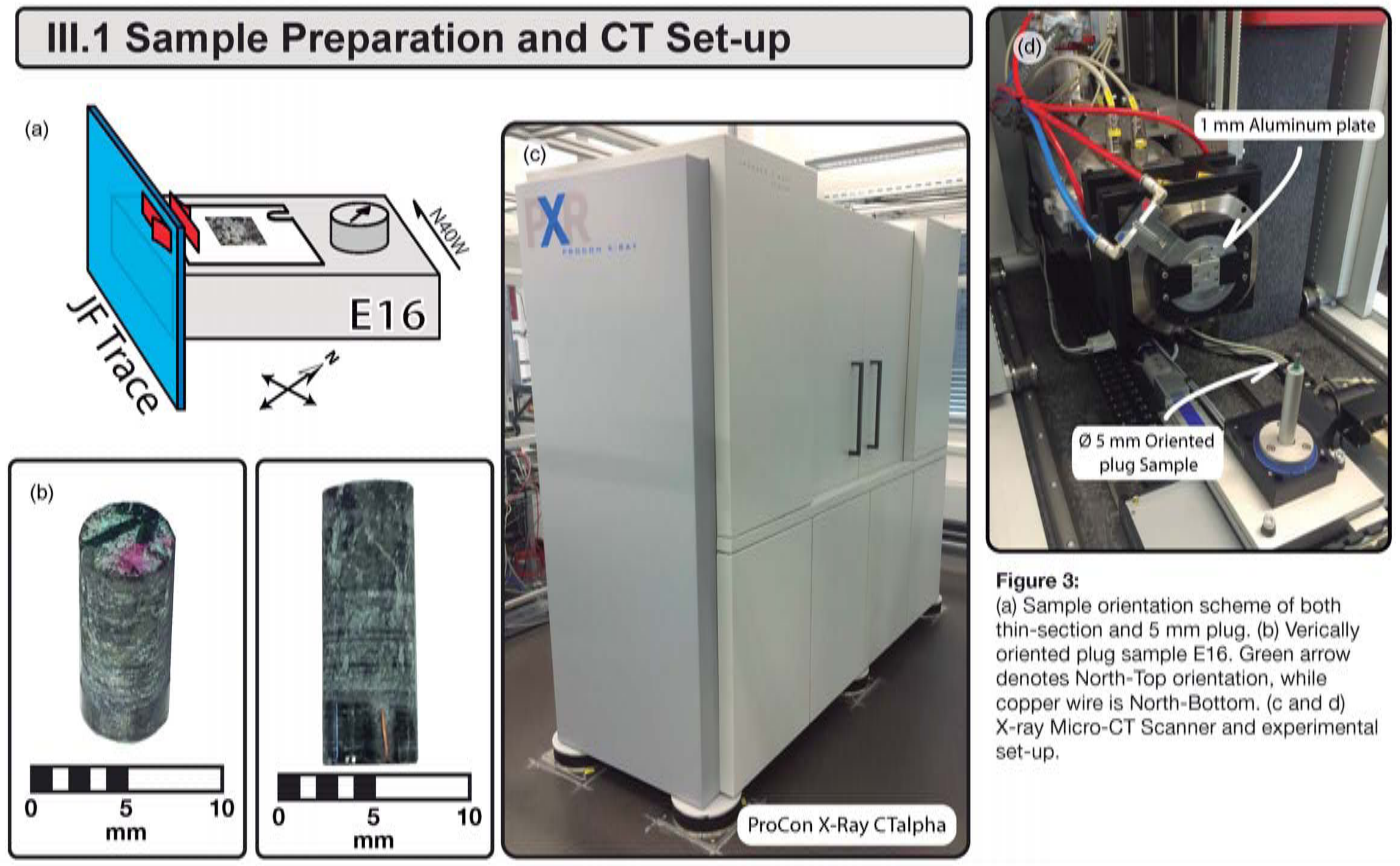

Figure 3:
(a) Sample orientation scheme of both thin-section and 5 mm plug. (b) Verically oriented plug sample E16. Green arrow denotes North-Top orientation, while copper wire is North-Bottom. (c and d) X-ray Micro-CT Scanner and experimental set-up.

IV. Microfracture Charaterization

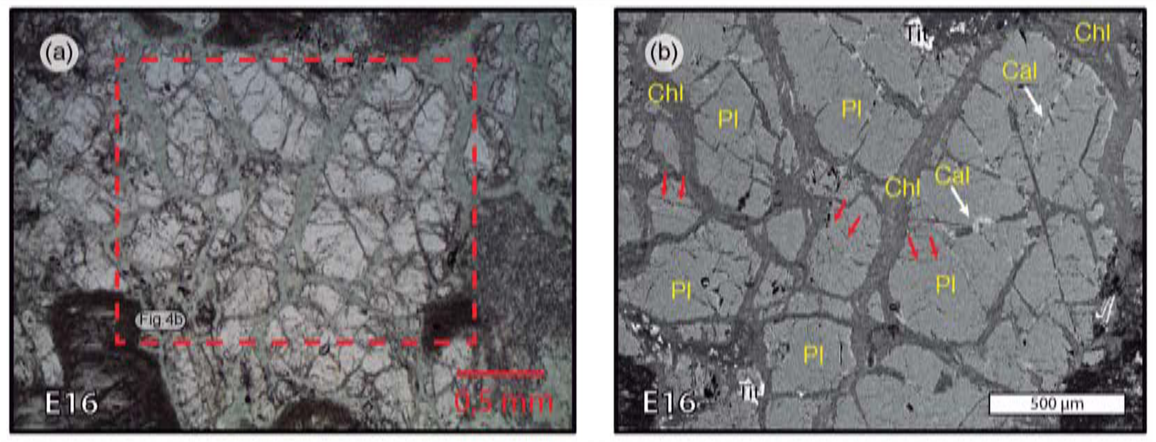

Figure 4:
(a) PPL Microphotograph of the chlorite-sealed extension microfractures.
(b) SEM-BSE Image showing in-situ fragmented rock matrix formed by sub-angular plagioclase (Pl) grains with no or little clast rotation cemented by chlorite and minor amounts of calcite. Open fractures are pointed by red arrows. White letters denotes sample name and distance from JF core.

V. Preliminary Results

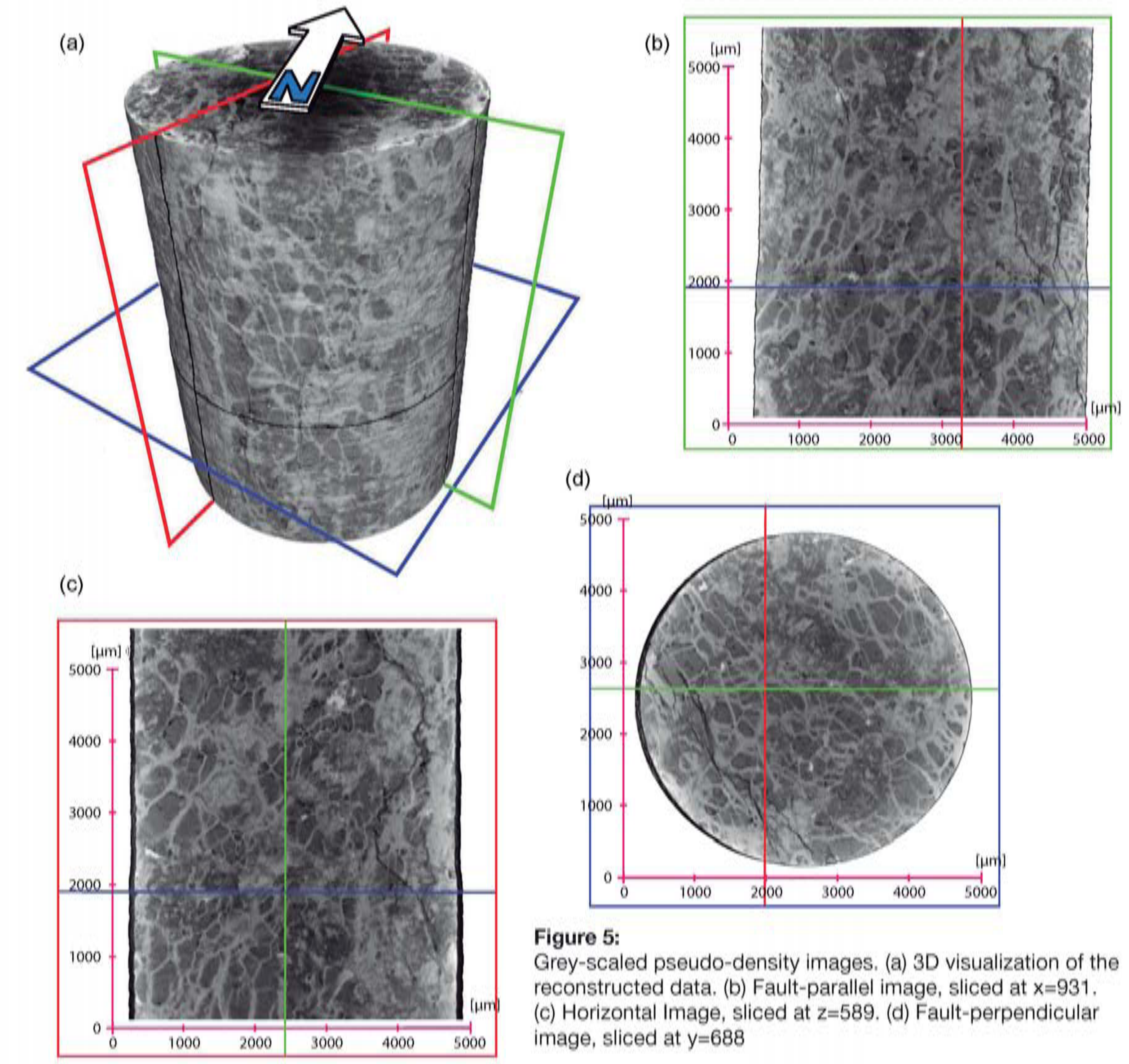

Figure 5:
Grey-scaled pseudo-density images. (a) 3D visualization of the reconstructed data. (b) Fault-parallel image, sliced at x=931. (c) Horizontal Image, sliced at z=589. (d) Fault-perpendicular image, sliced at y=688

VI. Future Work

Future work will be aimed in the images segmentation of the fault-related fracture mesh of a fixed Volume Of Interest (VOI; Figure 6), followed by the estimation of its hydraulic properties at the time of fracture sealing by means of simulation of fluid flow through the cracks using Lattice Boltzmann Methods.

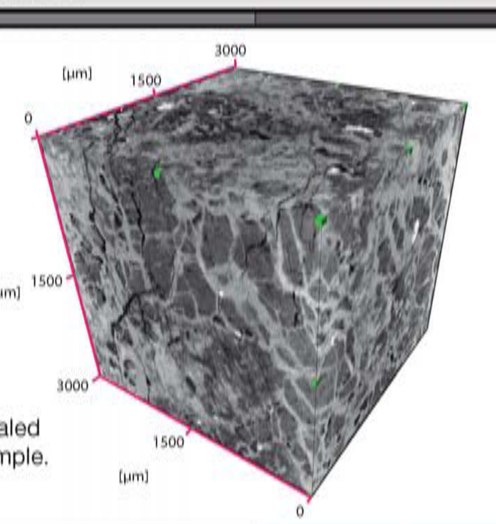

Figure 6:
3D visualization of the reconstructed data as a grey-scaled pseudo-density image of the VOI from the scanned sample. VOI dimensions are 3000 x 3000 x 3000 [μm]

VII. References

Annisofira and Latief. 2015. Proceedings World Geothermal Congress 2015
Baker et al. 2012. Lithos 148. 262–276.
Bultreys et al, 2016. Earth-Science Reviews 155. 93–128
Caine, J. et al. 1996. Geology; v. 24; no. 11; p. 1025–1028.
Cnudde and Boone, 2013. Earth-Science Reviews 123. 1–17
Cox, S. F. et al. 2001. Reviews in Economic Geology, 14, 1–24.
Cox, S. F. 2005. In Economic Geology 100th Anniversary Volume, pp. 39–75.
Faulkner, D. et al. 2010. Journal of Structural Geology. 32, 1557–1575.
Gueguen, Y. and Dienes, J. 1989. Mathematical Geology 21, 1 –13.
Gomila, et al. 2016. Journal of Structural Geology 83, 103-120.
Gueguen, Y., et al. 1996. Surveys in Geophysics 17: 245-263.
Ketcham and Carlson, 2001. Computers & Geosciences 27. 381–400
Kyle and Ketcham, 2014. Ore Geology Reviews 65 (2015) 821–839
Latief et al. 2014. Microscopy and Analysis 28(2):13-17.
Lee, H.S., Cho, T.F. 2002. Rock Mechanics and Rock Engineering 35, 299–318.
Lespinasse, M., et al. 2005. Chemical Geology 758 223, 170–178.
Mitchell, T.M. and Faulkner, D. R. 2008. Journal of Geophysical Research - Solid Earth 113 (B11).
Mitchell, T.M. et al. 2011. Earth and Planetary Science Letters 308. 284–297
Sausse, J. et al. 2001. Tectonophysics 336 (1–4), 199–214.
Sibson, R.H. 2003. Bulletin of the Seismological Society of America, v. 93, no. 3, p. 1169–1178.
Veloso, E. et al. 2015. Tectonophysics 664, 244–255. doi:10.1016/j.tecto.2015.09.022
Woodcock, N.H. et al. 2007. Geological Society, London, Special Publications 270, 43–53.

Acknowledgement

This study was funded in part by FONDECYT project 1100464, by CONICYT DOCTORADO NACIONAL 21140021 and is a contribution to the CONICYT- BMBF International Scientific Collaborative Research Program Project PCCI130025/FKZ01DN14033 and the FONDAP-CONICYT Project 15090013.

Intrested in this work? Please feel free to visit for my latest information in this and other research.

This presentation participates in OSPP

Outstanding Student Poster & PICO Contest